Remote Sens. **2014**, *6*, 4061-4089; doi:10.3390/rs6054061

OPEN ACCESS

remote sensing

ISSN 2072-4292

www.mdpi.com/journal/remotesensing

Article

A Decade Long, Multi-Scale Map Comparison of Fire Regime Parameters Derived from Three Publically Available Satellite-Based Fire Products: A Case Study in the Central African Republic

Patrick H. Freeborn [1,*], Mark A. Cochrane [1] and Martin J. Wooster [2,3]

[1] Geographic Information Science Center of Excellence, South Dakota State University, Brookings, SD 57007, USA; E-Mails: mark.cochrane@sdstate.edu

[2] Earth and Environmental Dynamics Research Group, Department of Geography, King's College London, London WC2R 2LS, UK; E-Mail: martin.wooster@kcl.ac.uk

[3] NERC National Centre for Earth Observation, London WC2R 2LS, UK

* Author to whom correspondence should be addressed; E-Mail: patrick.freeborn@sdstate.edu; Tel.: +1-605-688-4787; Fax: +1-605-688-5227.

Received: 30 December 2013; in revised form: 23 April 2014 / Accepted: 24 April 2014 / Published: 2 May 2014

Abstract: Although it is assumed that satellite-derived descriptions of fire activity will differ depending on the dataset selected for analysis, as of yet, the effects of failed and false detections at the pixel level and on an instantaneous basis have not been propagated through space and time to determine their cumulative impact on the characterization of individual fire regime parameters. Here we perform the first ever decade long, multi-scale map comparison of fire chronologies and fire seasonality derived from three publicly available satellite-based fire products: the MODIS active fire product (MCD14ML), the ATSR nighttime World Fire Atlas (WFA), and the MODIS burned area product (MCD45A1). Results indicate that: (i) the agreement between fire chronologies derived from two dissimilar satellite products improves as fire pixels are aggregated into coarser grid cells, but diminishes as the number of years included in the time series increases; and (ii) all three datasets provide distinctly different portraits of the onset, peak, and duration of the fire season regardless of the map resolution. Differences in regional, long-term fire regime parameters derived from the three datasets are attributed to the unique capability of each sensor and detection algorithm to recognize geographical gradients, seasonal oscillations, decadal trends, and interannual variability in active fire characteristics and

burned area patterns. Since different satellite sensors and detection algorithm strategies are sensitive to different types of fires, we demonstrate that disagreements in fire regime maps derived from dissimilar satellite-based fire products can be used as an advantage to highlight spatial and temporal transitions in landscape fire activity. Given access to multiple, publically available datasets, we caution against describing fire regimes using a single satellite-based active fire or burned area product.

Keywords: fire occurrence; fire chronologies; fire seasonality; MODIS; (A)ATSR; active fire; burned area

1. Introduction

Mapping fire regimes is useful for understanding disturbance-vegetation-climate interactions, for assessing ecological integrity and ecosystem change, for identifying fire hazard and fire risk, for informing fire, fuels and resource management decisions, and for identifying gaps in knowledge about the spatiotemporal patterns of fire [1–3]. In general, fire regimes describe the role of landscape fires within an area over time, and under this broad definition, the fires' physical attributes are typically parameterized by fire frequency, size, season, intensity and type [4]. Characterizing fire regimes has historically been performed by analyzing field data such as charcoal records [5], fire-scar networks [6], fire occurrence databases [7], and time-series of fire perimeters traditionally referred to as fire atlases (e.g., [8]). Mapping fire regimes from these spatially limited datasets is typically performed by extrapolating fire history information across the landscape using classification schemes (e.g., [9]), statistical models [10], spatially explicit simulations [11,12], or any combination thereof [3]. However, given the time, cost, and limited coverage of field surveys, and the geostatistical issues associated with extrapolating spatial data [1,13], satellite images of active fires and burned areas are increasingly being used to monitor fire histories as they unfold [14].

Active fire detection strategies rely on increased infrared brightness temperatures to identify sub-pixel hotspots burning at the time of image acquisition [15,16], and burned area detection strategies identify changes in the pre- and post-fire surface reflectance that accompanies fuel consumption, the deposition of char and ash, and the alteration of vegetative cover [17]. Information about the timing and location of active fire (AF) and burned area (BA) pixels is stored in data files often referred to as "fire products." Active fire and burned area pixels are merely evidence of a fire, like a fire scar on a tree ring, and a single AF or BA pixel rarely represents accurately the full duration and spatial extent of a single fire. Instead, the accumulation of multiple AF and BA pixels represents multiple observations of the same fire through time and across the landscape.

Satellite-based AF and BA products have most often been used to characterize individual parameters within the overall context of a fire regime. For example, satellite-derived fire chronologies have been used to determine distributions of fire return intervals from which fire frequency can be calculated (e.g., [18–21]), and fire seasonality has been characterized using a variety of satellite-derived metrics including the peak [22], the mid-point [23,24], the length of fire period [25], the fire season duration [26], the core burning season [27,28], and the classification of early and late season fires [29,30].

Fewer studies have derived and consolidated multiple satellite-based parameters such as fire frequency, seasonality, size and intensity to map overall fire regime classes or pyromes (e.g., [24,26,31,32]).

Despite the increased use of publically available fire products, confident interpretations of satellite-derived fire regime parameters are hindered by the underlying limitations and caveats of detecting active fires and burned areas from spaceborne platforms. No satellite-based fire product is a perfect representation of the true landscape fire activity. Satellite-based fire products suffer from omission and commission errors due to imperfect sampling designs (e.g., infrequent and non-optimal overpass times, coarse spatial resolutions, ill-suited spectral band selection, *etc.*), imperfect detection algorithm strategies and sensitivities, and imperfect observation conditions (e.g., cloud and tree canopy cover). Omission and commission errors are typically quantified at the pixel level, and on an instantaneous basis in the case of AF products [33–36], and on a daily basis in the case of BA products [37–39]. At these spatiotemporal resolutions, omission errors represent the failure of a fire product to record a true fire located in a particular area at a specific time, and commission errors represent false detections of non-existent fires. Omission and commission rates are not universal. Rather detection rates have been shown to vary between satellite products, and between validation sites depending on active fire characteristics and burned area patterns, surrounding canopy cover, and atmospheric conditions at the time of the observation [33–40].

Even if a fire product fails to record an event at a specific time (e.g., during a morning observation when the fire is too small or not intense enough to be detected, or during an overcast day when the land surface is obscured by clouds), it is still possible for a fire product to contain a record of the same fire at a different time (e.g., if the same area is observed when burning and atmospheric conditions are more conducive to detection). Moreover, most interpretations of landscape fires are not performed at the pixel level or in near-real time. Instead AF and BA pixels are usually accumulated and analyzed at coarser spatiotemporal resolutions. As of yet, however, the cumulative effects of failed and false detections at the pixel level and on an instantaneous/daily basis have not been propagated through space and time to determine their aggregate impact on the characterization of regional, long-term fire regime parameters. Given the complex interactions between: (i) the true spatial and temporal variability of fire activity; (ii) the native spatiotemporal resolution of the raw fire products; and (iii) the spatiotemporal scale of the pixel aggregation process, the cumulative impact of AF and BA detection performance on the characterization of individual fire regime parameters may not be intuitive. Consequently, the variability in fire regime parameters derived from different, publically available satellite-based fire products remains unknown.

Rather than directly evaluating AF and BA detection performance, which has been the subject of previous studies (e.g., [33–40]), this work explores for the first time the potential of dissimilar satellite-based fire products to provide competing and/or synergistic descriptions of key fire regime parameters. We analyze three independent, publically available, 10-year long datasets: the Moderate Resolution Imaging Spectroradiometer (MODIS) monthly active fire product (MCD14ML), the (Advanced) Along Track Scanning Radiometer (ATSR) nighttime World Fire Atlas (WFA), and the MODIS burned area product (MCD45A1). Maps of annual fire occurrence and maps of the onset, peak and duration of the fire season are derived from each dataset and are compared across a variety of spatiotemporal scales since: (i) it is possible to derive these parameters from all three fire products; (ii) these parameters are most often used to describe fire regimes; and (iii) these parameters have been

derived and interpreted at spatial resolutions ranging from the pixel level to coarse grid cells. Here, comparisons between the satellite-derived fire regime parameters are performed as part of a case study designed to exploit a well-known gradient of fire behavior across the Central African Republic (CAR), one of the most fire-affected countries in Africa whose burning patterns have been the subject of a wide range of past studies [23,24,26,28–31,41–43].

In this work, we do not purport to characterize the "true" fire activity, nor do we attempt to identify the primary vegetative, climatic, and anthropogenic drivers of fire activity across the CAR. Furthermore, we do not directly compare concurrent and collocated AF pixel counts, nor do we relate AF pixel counts to burned area. Our intent is to purposely allow individual errors of omission and commission to propagate through the processing of the datasets to determine their cumulative effect on the derivation of fire regime parameters. Doing so enables the three satellite-based fire products to be compared at spatial and temporal scales more appropriate for characterizing regional, long-term fire regimes. In this manner, our goal is to identify where and when in the CAR the three satellite-derived fire regimes agree and/or disagree, and to examine the possible reasons for their agreement and/or disagreement. Readers interested in a traditional validation of AF and BA detection performance, including the quantification of omission and commission rates, or a direct comparison between the datasets on a per-pixel and instantaneous basis, should look elsewhere in the literature (e.g., [16,33–40]).

2. Methods

2.1. Datasets

The MODIS sensor—flown aboard NASA's Terra and Aqua satellites since December 1999 and May 2002 respectively—has collected images of the Earth's surface in 36 spectral bands ranging from 250 m to 1 km spatial resolution [44]. In combination, MODIS Terra and Aqua observe locations at the equator up to four times every 24 h (twice during the day and twice at night) with imaging frequencies increasing polewards [45,46]. The MODIS active fire detection algorithm identifies ~1 km pixels containing sub-resolution, high temperature targets by applying absolute, multi-channel, and contextual detection thresholds to coregistered 3.9 μm and 11.0 μm images [15,47,48]. Information about MODIS active fire pixels is made available in a variety of formats, ranging from 5-minute granules to monthly global climate modeling grids [48]. Here we analyze 10 years of the Global Monthly Fire Location Product (MCD14ML), which is an ASCII file summarizing the timing and location of all MODIS active fire pixels detected globally in a single month [49].

Active fire monitoring from ESA's ERS-2 and ENVISAT platforms was accomplished between November 1995 and December 2002 using ATSR, and from January 2003 to March 2012 using the Advanced ATSR (AATSR), respectively [16]. Nighttime observations occur at 5 day intervals along the equator, and two different nighttime active fire detection algorithms (ALGO1 and ALGO2) have been used to generate two versions of the WFA, both of which rely on fixed 3.7 μm brightness temperature thresholds. Due to better continuity in the ALGO1 product between the ERS-2 and ENVISAT missions, and a higher tolerance for omission errors rather than commission errors, Arino *et al.* [16] examined trends in global night-time AF pixel counts detected using only the ALGO1

algorithm. Following their rationale, we too analyze only the ALGO1 product which classifies night-time AF pixels based on brightness temperatures above the (A)ATSR saturation limit of 312 K [16].

Independent of the active fire product, MODIS also has the capability of recognizing burn scars after the passage of a fire front. The MODIS burned area detection algorithm identifies daily fire affected areas at 500 m spatial resolution by comparing an observed reflectance time-series with a modeled bi-directional reflectance distribution function [39]. The MODIS burned area product (MCD45A1) records the approximate day of burning in non-overlapping tiles each covering ~1200 km × 1200 km [39]. Although disseminated as tiles, the 500 m grid cells contained therein are referred to hereafter as "burned area pixels" for convenience.

2.2. The CAR as a Case Study Site

The Central African Republic (CAR) was selected as a case study site (Figure 1) according to the criteria recommended by the Global Observation of Forest Cover (GOFC) Fire Implementation team and the Committee on Earth Observing Satellites (CEOS) Land Product Validation (LPV) subgroup [50]. First, widespread fire activity in the region is considered a major driver of landscape dynamics and a significant source of atmospheric trace gasses and aerosols [23,51,52]. Second, due to geographic differences in vegetation type, landscape fragmentation and land use practices, a steep gradient of fire behavior in the CAR provides an opportunity to compare satellite-based fire products across a broad range of fire regimes but within a relatively narrow spatial domain [40]. Lastly, the CAR was selected as a case study site because a rich history of satellite-based AF and BA monitoring in the region (e.g., [23,24,26,28–31,41–43]) has provided insights into landscape fire activity that can be referenced during the interpretation of the more modern datasets.

Figure 1. Map of the Central African Republic (CAR) showing: (i) major road networks; (ii) locations of the western and eastern grid cells (labeled WGC and EGC) used to demonstrate two example fire seasons in Figure 2; and (iii) percent tree cover characterized according to the 500 m Global Land Cover Facility (GLCF) Version 3 of the Collection 4 Vegetation Continuous Field (VCF) product.

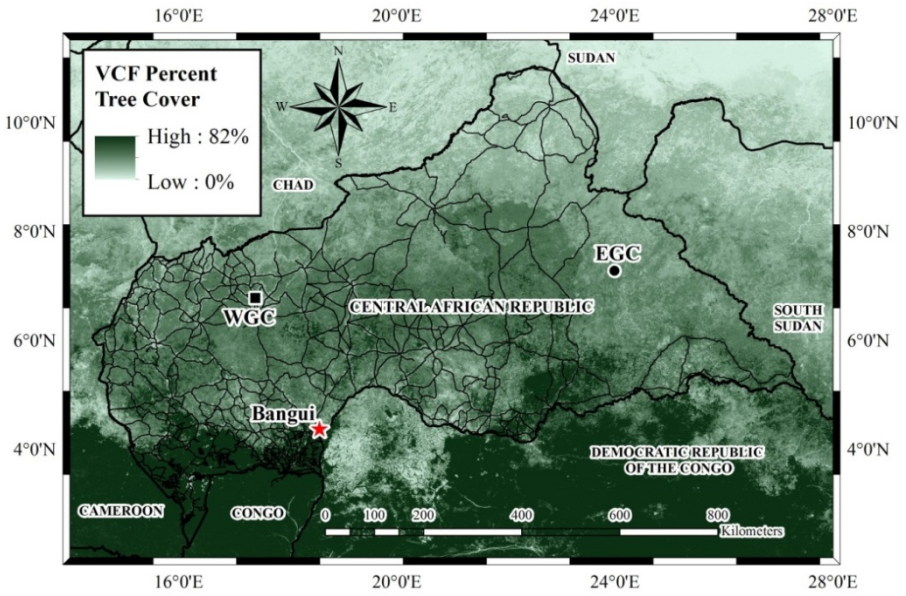

Figure 2. Normalized seasonal profiles of (**a**) MODIS active fire (AF) pixel counts and (**b**) cumulative distributions of MODIS AF pixel counts for two 0.05° grid cells at 16-day temporal resolution. Seasonal profiles are generated from 10 years of aggregated observations, and the locations of the example grid cells, referred to as the western and eastern grid cells (WGC and EGC), are shown in Figure 1. The 10th and 90th percentiles of the cumulative AF pixel counts are shown in (b) to demonstrate the "fire season duration" as determined in this work.

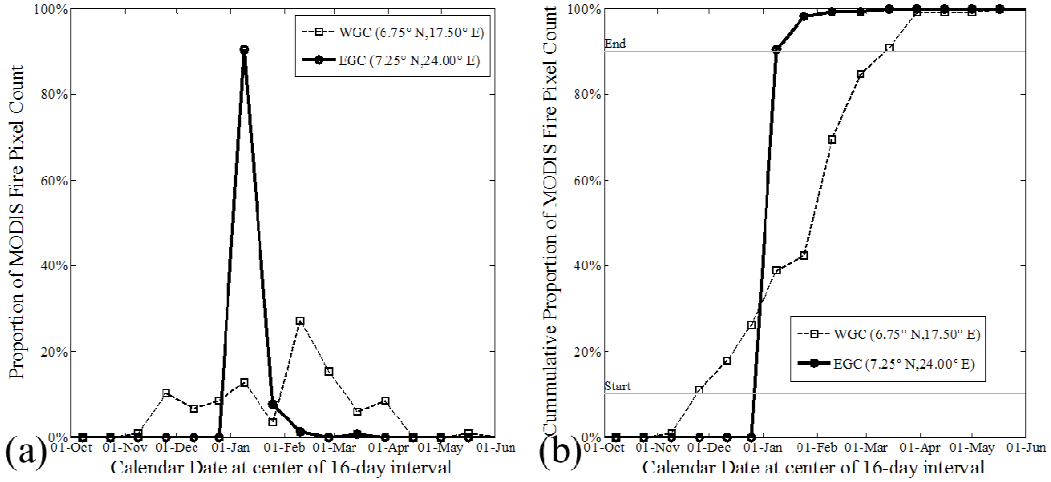

2.3. Annual Fire Occurrence and Fire Chronologies

Fire frequency is one component of a fire regime, and is classically defined as the inverse of the mean fire return interval [10]. The mean fire return interval itself is defined as the mean number of years between successive fires at a specific point on the landscape or within a specified area [10]. Since a pixel inherently contains spatially integrated spectral information, we are limited to characterizing fire regimes within specified areas, in this case grid cells, which likely subtend multiple AF and BA pixels per year. To derive the mean fire return interval for a particular grid cell, therefore, requires a time-series of annual fire occurrence. Annual fire occurrence is defined here as the detection of at least one fire pixel within a grid cell during the year. Much like the presence or absence of a fire scar on a tree-ring, annual fire occurrence within a grid cell is a binary metric such that either a fire occurred during the year or it didn't. The intent of a time-series of annual fire occurrence—or a fire chronology—is not to record the absolute number of AF or BA pixels detected within an area, nor is it intended to count the number of "real" fires that occurred within an area over time. Rather, the purpose of a fire chronology is to document the individual years in which there is evidence of at least one fire. Results here are restricted to comparisons and interpretations of annual fire occurrence and fire chronologies due to the limitations of confidently estimating mean fire return intervals and fire frequencies from such brief datasets [53].

Maps of annual fire occurrence were generated at 10 spatial resolutions by sorting AF and BA pixels from each of the three datasets into grid cells ranging from 0.05° to 0.5° in size (*i.e.*, ranging from ~5.5 km to ~55 km at latitudes in the CAR). For each fire product, and for each grid cell resolution, ten binary maps of annual fire occurrence (one for each year between 2002 and 2012) were created to indicate whether a fire was detected in a grid cell at any time during a "fire year." To avoid

splitting a continuous fire season into two calendar years, the start and end of the "fire year" in the CAR was defined to coincide with a minimum of fire activity on the 20th of July as determined from the MODIS active fire product.

The MODIS active fire product was considered as the reference, and comparisons of annual fire occurrence were made between the MCD14ML and WFA datasets, and between the MCD14ML and MCD45A1 datasets. Although selection of the MODIS AF product as the reference could be considered somewhat arbitrary, a preliminary evaluation indicated that the MODIS AF product was far more likely to detect evidence of fires from the beginning to the end of the fire season, and throughout the CAR, thus making this a more suitable reference in our comparisons. The agreement between any two maps of annual fire occurrence produced for the same year and at the same spatial resolution, but derived from dissimilar datasets, was quantified according to the proportion of grid cells in the CAR where: (i) both fire products recorded at least one fire pixel during the year; or (ii) neither fire product recorded a fire pixel during the year.

Decade long fire chronologies in each grid cell were generated from time series of annual fire occurrence. Examples of fire chronologies are presented in Table 1 for a single 0.05° grid cell located in the east of the CAR labelled as "EGC" in Figure 1. Note that although Table 1 reports annual AF and BA pixel counts, the detection of more than a single fire pixel in a grid cell during a fire year is essentially irrelevant to the construction of a chronology of annual fire occurrence. For these examples, only the MODIS AF (MCD14ML) and MODIS BA (MCD45A1) datasets yielded the same fire chronology in the EGC. Again, maps of fire chronologies were compared using the MODIS active fire product as the reference. The agreement between any two maps of fire chronologies produced at the same spatial resolution but derived from dissimilar datasets was quantified according to the proportion of grid cells in the CAR that shared an identical time-series of annual fire occurrence.

Table 1. Chronologies of annual fire occurrence derived from the MODIS active fire product (MCD14ML), the (A)ATSR active fire product (WFA), and the MODIS burned area product (MCD45A1) for a single 0.05° grid cell identified as the eastern grid cell (EGC) shown in Figure 1. A plus sign "+" indicates that a dataset recorded evidence of a fire in a particular year, and a negative sign "–" indicates that a dataset did not record evidence of a fire in particular year. Since only annual fire occurrence contributes to the classical definition of a fire regime, only this parameter (and not AF or BA pixel counts) is compared between the datasets.

	Fire Year for Eastern Grid Cell, EGC (7.25°N, 24.00°E)									
	02/03	**03/04**	**04/05**	**05/06**	**06/07**	**07/08**	**08/09**	**09/10**	**10/11**	**11/12**
MCD14ML AF Pixel Count	5	11	8	9	12	8	8	13	12	12
MCD14ML Chronology of Annual Fire Occurrence	+	+	+	+	+	+	+	+	+	+
(A)ATSR WFA AF Pixel Count	0	0	0	0	0	0	0	1	0	1
(A)ATSR WFA Chronology of Annual Fire Occurrence	–	–	–	–	–	–	–	+	–	+
MCD45A1 BA Pixel Count	129	108	107	141	138	104	139	134	129	92
MCD45A1 Chronology of Annual Fire Occurrence	+	+	+	+	+	+	+	+	+	+

2.4. Fire Seasons

The seasonality of fire activity is another component of a fire regime. In this work, all MODIS active fire pixels, (A)ATSR active fire pixels, and MODIS burned area pixels were assigned to a day of the year (1–365, or 1–366 for leap years), and were sorted into 16-day compositing periods coinciding with the 8-day schedule of the MODIS Climate Modeling Grid (CMG) fire product [49]. For each fire product, and in each grid cell, the 10 seasonal profiles of fire pixel counts (*i.e.*, one for each year) were summed to create a single, aggregated seasonal profile of AF or BA detections representative of the entire decade-long study period. All ten years of data are used to generate a single "aggregate" or "mean" seasonal profile in each grid cell since fire regimes are, by definition, intended to describe fire activity over time periods longer than one fire return interval. The implications of constructing an "aggregate" or "mean" seasonal profile from 10 years of data are addressed in the Discussion (Section 4).

Figure 2 illustrates examples of aggregated seasonal profiles for two separate 0.05° grid cells. These two grid cells exhibit distinctly different seasonal profiles of fire activity. The western grid cell (WGC), located near the city of Bossangoa (Figure 1), is characterized by a broad seasonal profile of AF pixels detected from October to May, most likely due to the agricultural burning of small farms and pastures [54]. In contrast, the eastern grid cell (EGC), located near the South Sudan border (Figure 1), is characterized by a concentration of AF pixels primarily detected within a 16-day compositing period, most likely due to long, continuous, free-burning fire fronts set by hunters that propagated through the grid cell over the course of a few days [54].

As previously mentioned, a variety of satellite-based remote sensing variables have been developed to characterize fire seasonality, each of which has its' own definition and its own method of calculation (e.g., [22–30]). Here, fire seasonality is characterized according to the cumulative distribution of fire pixels detected within a grid cell [24,26,31]. Due to differences in the spatial and temporal resolutions of the observations, and due to the strong gradient of fire activity across the CAR, it is inappropriate to define the fire season in each grid cell using a universal threshold based on an absolute count of AF or BA pixels. A relative threshold is used instead, and for all three fire products, the start and end of the fire season are identified as the first compositing period in which the cumulative number of AF or BA pixels equals or exceeds 10% and 90% of the aggregate total in each grid cell, respectively (Figure 2b). The peak of the fire season is identified as the compositing period containing the maximum fire pixel count; the fire season duration (FSD) is determined according to the number of compositing periods between the 10th and 90th percentiles; and a grid cell is assigned a null value if a fire pixel was not recorded during the year. The consequences of defining the fire season according to percentiles of the cumulative distribution are addressed in the Discussion (Section 4).

Ten maps of fire seasonality in the CAR were generated for each satellite-based fire product: one for each of the ten aforementioned spatial resolutions. The agreement between any two fire season maps generated at the same spatial resolution—but derived from two different datasets—was assessed using an overall accuracy metric, P, representing the percentage of grid cells in the CAR where both datasets: (i) detected a fire pixel; and (ii) yielded an identical start, peak, or end date depending on the parameter being assessed. The former criteria are necessary since a fire season can only be characterized in a grid cell if an AF or BA pixel is detected during the study period. Hence fire seasons

are only compared between the datasets for grid cells containing at least one fire pixel recorded in both datasets, which is later shown to occur in the majority of CAR grid cells at resolutions coarser than 0.1°. Again the MODIS active fire product is used as the reference, and a consistent nomenclature is used to denote the agreement between any two fire season maps derived from dissimilar fire products. The subscripts *AFAF* and *AFBA* indicate comparisons between the MODIS and (A)ATSR active fire products, and between the MODIS active fire and MODIS burned area products, respectively. The superscripts *start*, *peak*, *end*, and *fsd* refer to the parameter being assessed. For example, P_{AFAF}^{fsd} refers to the percentage of grid cells in the CAR containing a fire pixel recorded by the MCD14ML and WFA active fire products that were also assigned an identical fire season duration.

3. Results

3.1. Comparisons of Annual Fire Occurrence

Binary maps of annual fire occurrence in the CAR derived from the MODIS (MCD14ML) and (A)ATSR (WFA) active fire datasets showed poor agreement in 2002 & 2003 at the finest spatial resolution. Only 13% of the 0.05° grid cells in the CAR contained (i) both a MODIS and an (A)ATSR active fire pixel; or (ii) neither a MODIS nor an (A)ATSR active fire pixel (Figure 3a). Where the two AF products disagree, 87% of the 0.05° grid cells in the CAR contained at least one MODIS AF pixel detected during the year but no (A)ATSR AF pixel. Conversely, less than 1% of the 0.05° grid cells in the CAR contained at least one (A)ATSR active fire pixel detected during the year but no MODIS AF pixel. Hence disagreements in maps of fire occurrence for individual years are overwhelmingly attributed to the presence of MODIS AF pixels and the absence of (A)ATSR AF pixels. Part of the disagreement is due to differences in the sensor and detection algorithm sensitivities [16]; however part of the disagreement is due to non-simultaneous observation times. In the CAR, the (A)ATSR WFA product is generated from about 5 or 6 observations per month, and only at night when fires are generally far less prevalent across most of Africa [55]. In contrast, the MODIS AF product makes use of both daily daytime and nighttime observations, including an early afternoon MODIS Aqua overpass which is close to the diurnal peak in fire activity [55]. Despite differences in detection performance and observation times, there is an increased likelihood that both MODIS and (A)ATSR will detect an AF pixel within the same area as grid cells expand to capture more events. Consequently map agreements improve as fire pixels are aggregated into coarser grid cells. For example, the MODIS- and ATSR-derived maps of fire occurrence in 2002 & 2003 agreed across 81% of the CAR if AF pixels were accumulated into 0.5° grid cells (Figure 3a).

Comparisons of annual fire occurrence derived from the MODIS active fire (MCD14ML) and MODIS burned area (MCD45A1) datasets fared much better. In 2002 & 2003, for example, maps of annual fire occurrence derived from the MODIS AF and BA products agreed in 76% of the 0.05° grid cells in the CAR (Figure 3b). Where the two products disagreed, 24% of the 0.05° grid cells in the CAR contained at least one MODIS AF pixel detected during the year but no MODIS BA pixel. Conversely, less than 1% contained at least one MODIS BA pixel detected during the year but no MODIS AF fire pixel. Hence map disagreements are again attributed to the presence of MODIS AF pixels and the absence of MODIS BA pixels. As with comparisons between the MODIS and (A)ATSR

AF pixels, map agreements improved as grid cell sizes expand, such that the map agreement between the MODIS AF- and MODIS BA-derived annual fire occurrence in 2002 & 2003 exceeded 98.0% for grid cells larger than 0.35° (Figure 3b).

Figure 3. Comparison of annual fire occurrence maps in the CAR for individual years during the study period. Comparisons between maps derived from the MCD14ML and WFA active fire products (**a**), and between the MCD14ML active fire product and MCD45A1 burned area products (**b**), are based on the proportion of grid cells in the CAR that contained: (i) at least one fire pixel recorded in both datasets; or (ii) no fire pixels recorded in either dataset. Each temporal profile (solid line) coincides with a particular grid cell resolution, ranging from 0.05° to 0.5° in size.

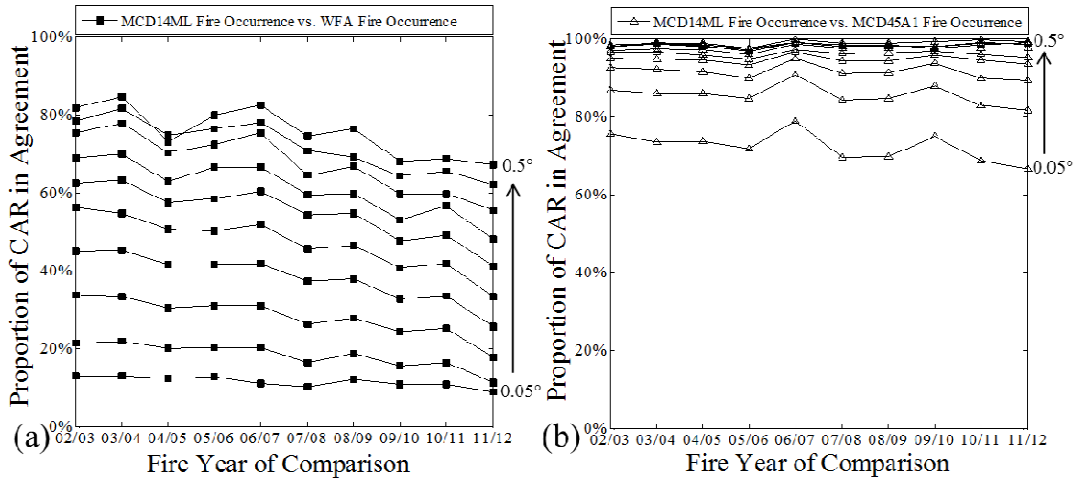

Comparing individual maps of annual fire occurrence for the remaining years in the study period revealed a slightly decreasing trend in the agreement between datasets through time (Figure 3a,b). For example, at 0.25° grid cell resolution, the MCD14ML and WFA active fire datasets agreed across 56% of the CAR in 2002 & 2003, but only agreed across 33% of the CAR in 2011 & 2012 (Figure 3a). Likewise at 0.05° grid cell resolution, the MODIS active fire and burned area datasets agreed across 76% of the CAR in 2002 & 2003, but agreed across only 67% of the CAR in 2011 & 2012 (Figure 3b). Decadal trends in the agreement between the datasets can be attributed to changes in active fire characteristics and burned area patterns. Over the course of a decade in the CAR, the mean fire radiative power (FRP) measured by MODIS decreased ~0.63 MW per year (Figure 4a); the proportion of night time AF pixels detected by MODIS decreased ~0.24% per year (Figure 4a); and the mean BA cluster size detected by MODIS decreased ~36.5 ha per year (Figure 4b). A decrease in the size or intensity of subpixel combustion components, as indicated by a decreasing trend in the mean FRP, would hinder the active fire detection performance of both MODIS and (A)ATSR, whilst a decrease in the proportion of night time fire activity would have a greater impact on the capability of (A)ATSR to detect evidence of a fire in a given location. Although burn scars surrounding active fire pixels could influence the measurement of background brightness temperatures, and thus influence the detection of active fires, it is more likely that a decreasing trend in the mean cluster size of BA pixels is indicative of more patch-like agricultural and pastoral burning practices, or possibly a shift in fire activity into areas with greater tree canopy cover, both of which are more difficult to detect based on changes in surface

reflectance alone [19,39]. Given that both the (A)ATSR active fire product and the MODIS burned area product indicate a decreasing trend in biomass burning across the CAR, and given that these results agree with a decreasing trend in burned area found in the northern hemisphere of Africa by Giglio *et al.* [56] using a different MODIS burned area detection algorithm [57], we suggest that changes in measured active fire characteristics and burned area patterns (Figure 4) are less attributed to drifts in instrument responses, and more attributed to a genuine shift in the timing, intensity, and extent of true fire activity.

Figure 4. Decadal trends in (**a**) the mean FRP and proportion of total active fire pixels detected at night; and (**b**) mean burned area cluster size measured by MODIS Terra and Aqua across the CAR between 2002 and 2012.

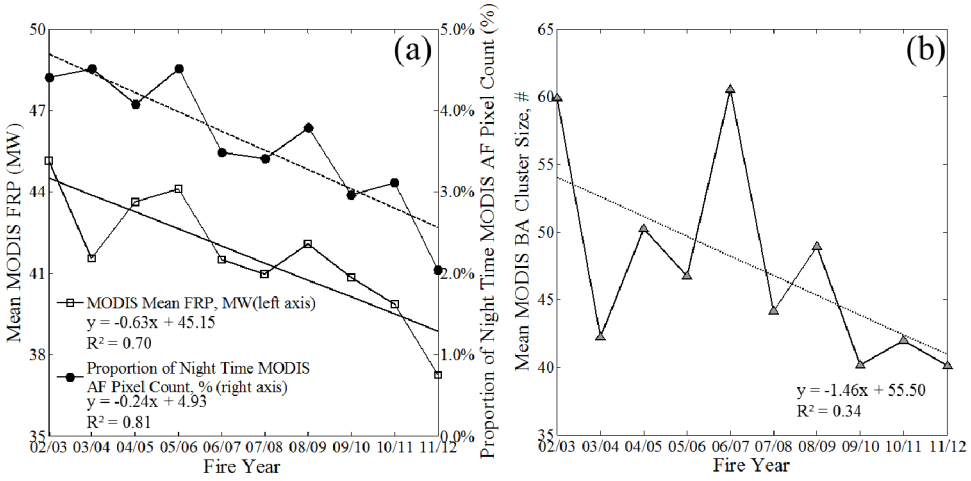

Transitions in the timing, intensity, and spatial extent of landscape fires (Figure 4) can have a negligible or a substantial effect on the characterization of annual fire occurrence from satellite observations depending on the magnitude of the change and the sensitivity of the detection algorithm to the change. For example, the proportion of 0.05° grid cells in the CAR that contained at least one MODIS active fire pixel detected annually remained relatively constant during the decade, such that between 93% and 95% of the area in the CAR was within ~17 km of a fire (Figure 5a). In contrast, the WFA active fire product and the MCD45A1 burned area product captured a decreasing trend in annual fire occurrence (Figure 5b,c). Ultimately, differences in the decadal trends of annual fire occurrence derived from each individual dataset shown in Figure 5 contribute to the decreasing trends in agreement between the datasets shown in Figure 3.

Locations where the fire products agreed and disagreed with respect to annual fire occurrence were not uniformly distributed across the CAR. Maps at 0.05° grid cell resolution depicting where the fire products agreed only for the March 2002 fire season (Figure 6a), and where the fire products agreed in any year during the study period (Figure 6b) highlight four distinct regions in the CAR:

(1) In the eastern and northeastern deciduous woodlands and shrublands of the CAR, particularly in the Haut-Mbomou prefecture along the border with South Sudan, all three datasets more often detect a fire pixel in the same grid cell in the same year. Here the agreement in annual fire occurrence derived from the MODIS and (A)ASTR active fire products is attributed to a coupling between the nighttime revisit schedule of both sensors and the typical fire behaviour in

the region, characterized by long, continuous, free-burning fire fronts that propagate across uninterrupted landscapes and persist into the night [54]. As a result of this fire behaviour, large, spatially contiguous patches of char and ash are also identifiable by the MODIS burned area detection algorithm.

Figure 5. Decadal trends in annual fire occurrence characterized according to the proportion of 0.05° grid cells in the CAR that contained at least one fire pixel recorded in (**a**) the MODIS active fire product; (**b**) the (A)ATSR nighttime world fire atlas; and (**c**) the MODIS burned area product. Trends in annual fire occurrence coincide with a transition in measured active fire characteristics and burned area patterns (Figure 4), and differences in these trends contribute to the reduced agreement between the datasets towards the end of the study period (Figure 3).

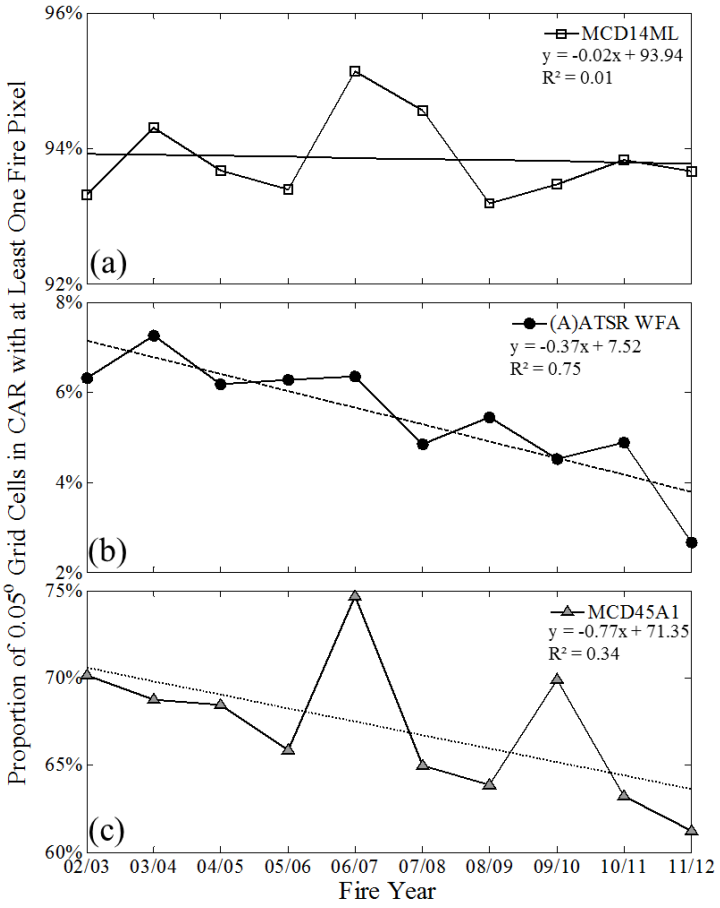

(2) All three datasets tend to agree in the extreme southwest prefecture of Sangha-Mbaéré where neither sensor detected an AF or BA pixel during the 10 year study period. These densely forested areas are unlikely to have experienced substantial amounts of fire. If, however, fires did occur in these the tropical semi-evergreen forests [58], then strong attenuation and obscuration by the substantial overlying canopy cover (see Figure 1) most likely prevented MODIS and (A)ATSR from detecting both the fire emitted thermal radiance as well as the burn scar.

(3) In the west-central prefectures, the daytime revisit schedule of MODIS offers opportunities unavailable to (A)ATSR to detect short-lived agricultural fires that are typically lit in the morning and do not burn into the night. Although the MODIS AF and BA detection algorithms

tend to agree in this region, it is also possible for evidence of smaller agricultural fires [54] to be missed by the MODIS burned area detection algorithm [39].

(4) In the east-central and southeast prefectures composed of forest/savanana mosaics and closed evergreen lowland forests, both "point-like" and "medium sized" fires burning during the day [54] are detectable using the MODIS infrared channels. However these fires extinguish or subside enough to remain undetected by (A)ATSR at night. In contrast to the small agricultural fires in the west, it seems more likely that MODIS fails to detect burned areas in these locations due to obscuration of the forest floor by tree canopy cover (see Figure 1).

Figure 6. Locations where the MODIS active fire (MCD14ML), the (A)ATSR nighttime world fire atlas (WFA), and the MODIS burned area (MCD45A1) datasets agreed in terms of annual fire occurrence. Shown in (**a**) are the locations where the datasets agreed only for the 2002/03 fire season, and shown in (**b**) are the locations where all three datasets agreed in any year during the study period.

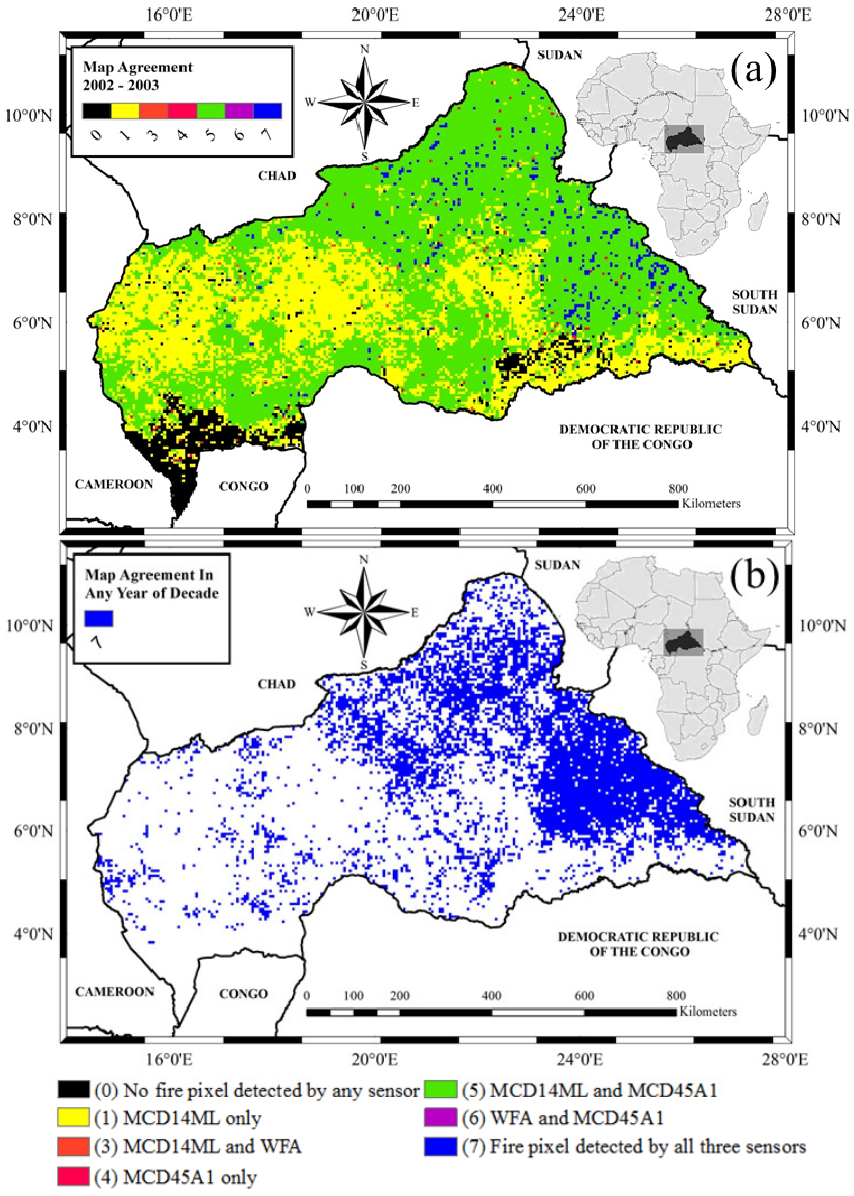

Interannual variability in the agreement between the datasets (Figure 3) is due—in part—to the fact that spatial patterns in the agreement between the datasets are not consistent over time. For example, differences in the pattern of blue grid cells between Figures 6a,b illustrates that it is possible for all three datasets to agree in different locations across the CAR from year to year. In general, however, all three datasets are more likely to agree in the eastern half of the CAR where long duration fires with long fire fronts and extensive burned areas are more likely to be detected regardless of the satellite sensor, the timing of the observation, or the detection algorithm strategy or sensitivity.

3.2. Comparisons of Fire Chronologies

The propensity of the MODIS (MCD14ML) and (A)ATSR (WFA) active fire datasets to record identical fire chronologies was assessed by expanding the number of years used in the comparison. Over two years between July 2002 and July 2004, the MCD14ML and WFA datasets recorded identical fire chronologies in 5% of the 0.05° grid cells in the CAR (Figure 7a). As the number of years included in the time-series increased, the agreement between fire chronologies decreased such that over the entire 10 year study period, the two AF products recorded identical fire chronologies in only 1% of the 0.05° grid cells in the CAR (Figure 7a). Similar to comparisons of fire occurrence for individual years, Figure 7a also demonstrates that the agreement between fire chronologies improves as AF pixels are accumulated into coarser grid cells. For instance, the two AF products yielded identical, decade long fire chronologies in 42% of the 0.5° grid cells in the CAR (Figure 7a).

Figure 7. Comparisons between fire chronologies derived from (**a**) the active fire (AF) datasets (MCD14ML and WFA); and (**b**) the MODIS AF dataset (MCD14ML) and the MODIS burned area (BA) dataset (MCD45A1). Comparisons are based on the proportion of grid cells in the CAR where both fire products recorded an identical 10 yr time-series of annual fire occurrence (e.g., see Table 1 for an example of a fire chronology in a single grid cell). Results demonstrate that the agreement between fire chronologies improves for coarser grid cell resolutions, but diminishes as the number of years included in the time-series increases.

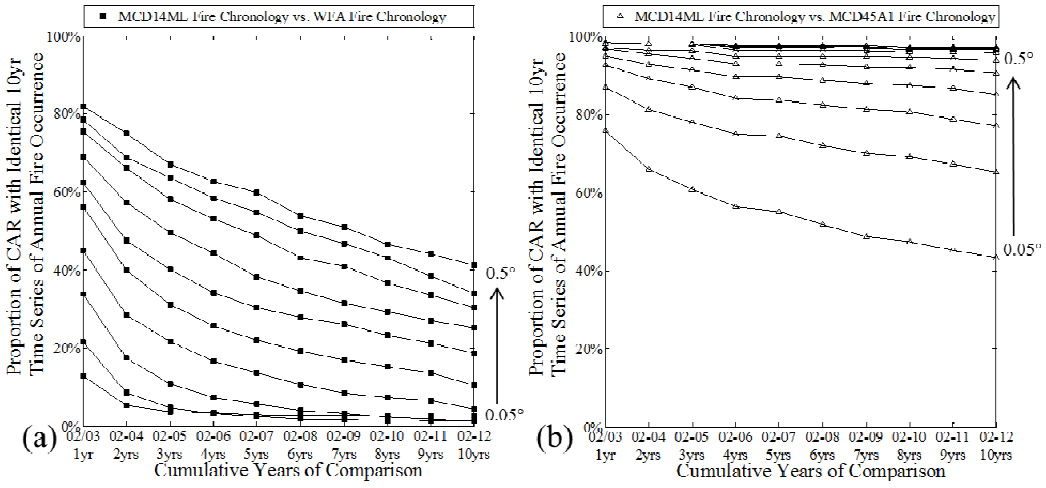

Likewise, whilst maps of fire occurrence derived from the MODIS active fire (MCD14ML) and burned area (MCD45A1) datasets show considerable agreement for any one year, the agreement in fire

chronologies is reduced as more years are included in the time-series (Figure 7b). For example, after 10 years, the agreement between the MODIS AF- and BA-derived fire chronologies reduces from 76% to 41% at the finest 0.05° spatial resolution. Disagreements in longer-term fire chronologies, however, are mitigated as fire pixels are accumulated into larger grid cells. Over the course of 10 years, for example, the MODIS AF and MODIS BA datasets yield identical fire chronologies in 97% of the 0.5° grid cells in the CAR.

As the time sequence of annual fire occurrence expands from one to 10 years, fire chronologies derived from the three different datasets agree in fewer and fewer grid cells across the CAR for two reasons. First, due to shifts in measured active fire characteristics and burned area patterns (Figure 4), which in turn affected the extent of annual fire detections (Figure 5), annual fire occurrence maps derived from the three datasets showed less and less agreement towards the end of the study period (Figure 3). As a consequence, disagreements in fire chronologies are more likely to be attributed to discrepancies in the characterization of annual fire occurrence between the datasets near the end of the study period. And second, in the absence of decadal trends, interannual variability in the timing, intensity, and spatial extent of fire activity could induce a disagreement in the detection of annual fire occurrence for any one year during the study period. Hence, due to interannual variability, it is possible for the agreement in fire chronologies to be disrupted at any time during the study period. In combination, these two artifacts (*i.e.*, decadal trends and interannual variability in the detection of annual fire occurrence) leads to the decreased agreement in satellite-derived fire chronologies as more years are cumulatively included in the time-series.

Again, the locations where the three fire products agree and disagree in terms of fire chronologies are not randomly distributed across the CAR. In general, map agreements in fire chronologies (Figure 8a,b) largely correspond to map agreements in annual fire occurrence (Figure 6a,b). Since the agreement in fire chronologies derived from the MODIS active fire and burned area products (Figure 8b) exhibits spatial patterns similar to the map of tree canopy cover (Figure 1), we stratified comparisons based on the 500 m Global Land Cover Facility (GLCF) Version 3 of the Collection 4 Vegetation Continuous Field (VCF) product [59]. Results indicate that the MODIS AF- and MODIS BA-derived fire chronologies agreed across 60% to 80% of the CAR in locations with tree cover less than 25% (Figure 9). Above 25% tree cover, however, the MODIS AF product overwhelmingly detects fires in more years than the MODIS BA product such that there is little (if any) agreement in grid cells with 70%–80% tree cover. At these forested locations, MODIS is more apt to detect the thermal radiance emitted by active fires burning under moderate tree cover since burned area detection algorithms are challenged to discern changes in surface spectral reflectance beneath the canopy [19,39]. Interestingly, the MODIS AF and MODIS BA detection strategies agree more consistently above 80% tree cover where the MCD14ML and MCD45A1 datasets yield identical fire chronologies in 43% of 0.05° grid cells in the CAR. Grid cells with the greatest tree canopy cover are mainly located in the extreme southwest prefecture of Sangha-Mbaéré where MODIS did not detect a single AF or BA pixel during the entire 10 year study period.

Figure 8. Maps of the agreement (in years; at 0.05° grid cell resolution) between fire chronologies derived from (**a**) the MODIS active fire product (MCD14ML) and the (A)ATSR nighttime world fire atlas (WFA); and (**b**) the MCD14ML active fire product and the MODIS burned area product (MCD45A1). A value of "10" (red) indicates that both satellite products generated an identical 10 year sequence of annual fire occurrence. A value of "0" (dark blue) indicates that annual fire occurrence derived from the dissimilar products disagreed in every year.

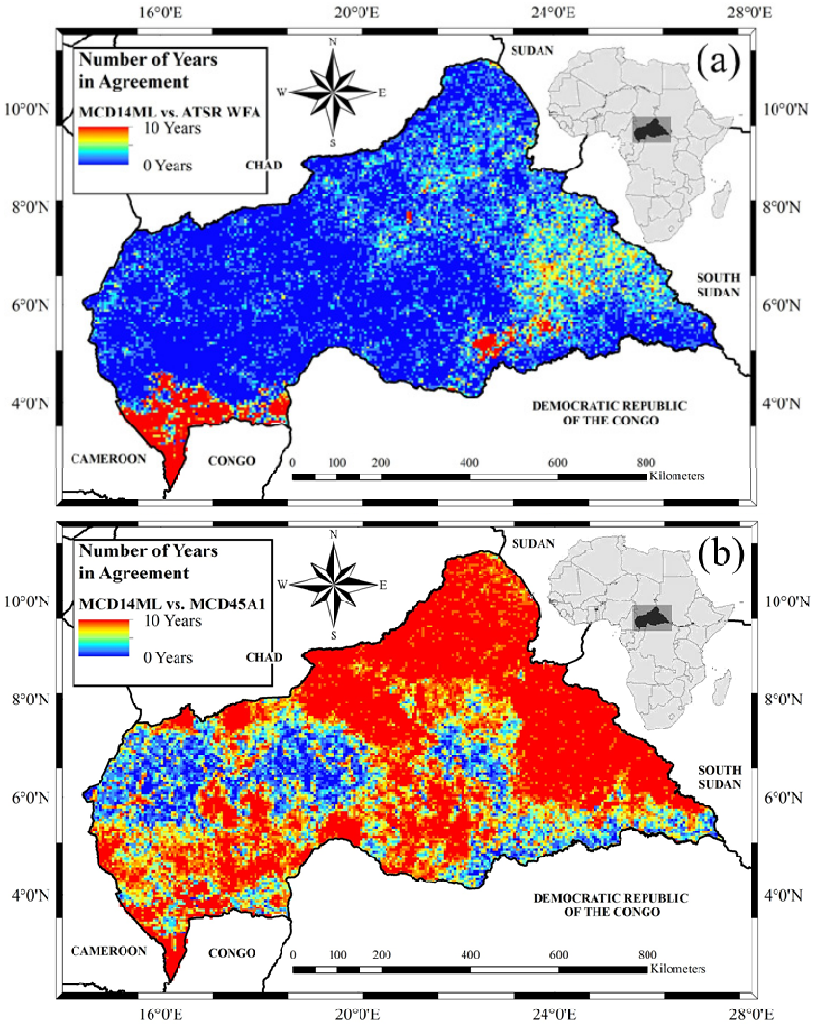

3.3. Comparisons of Fire Seasons

Maps of the fire season in the CAR determined from ten years of aggregated MODIS AF pixels are shown in Figure 10. Despite a general north-to-south progression of fire activity that coincides with the seasonal migration of the ITCZ and associated rainfall patterns [51,60], latitudinal bands across the CAR exhibit distributions of fire seasonality. This is partly explained by massive fire fronts driven by Harmattan winds that spread from South Sudan southwest into the CAR. Furthermore, whilst intra-latitudinal variations in the fire season can be attributed to ignition patterns, which are overwhelmingly determined by land use practices [29], the local microclimate nevertheless governs site-specific moisture contents and limits when fuels will ignite and carry a spreading fire. Whereas finer fuels exposed to the sun and wind dry out sooner and become flammable earlier in the year, greater canopy cover shelters heavier

fuels from insolation, maintains higher relative humidities, reduces windspeeds, and therefore prolongs the time it takes fuels to cure and permit an ignition to kindle and propagate.

Figure 9. Comparisons of fire chronologies at 0.05° grid cell resolution derived from ten years of the MODIS active fire (MCD14ML) and MODIS burned area (MCD45A1) datasets, expressed as a function of median tree canopy cover characterized using the Vegetation Continuous Field (VCF) product [59].

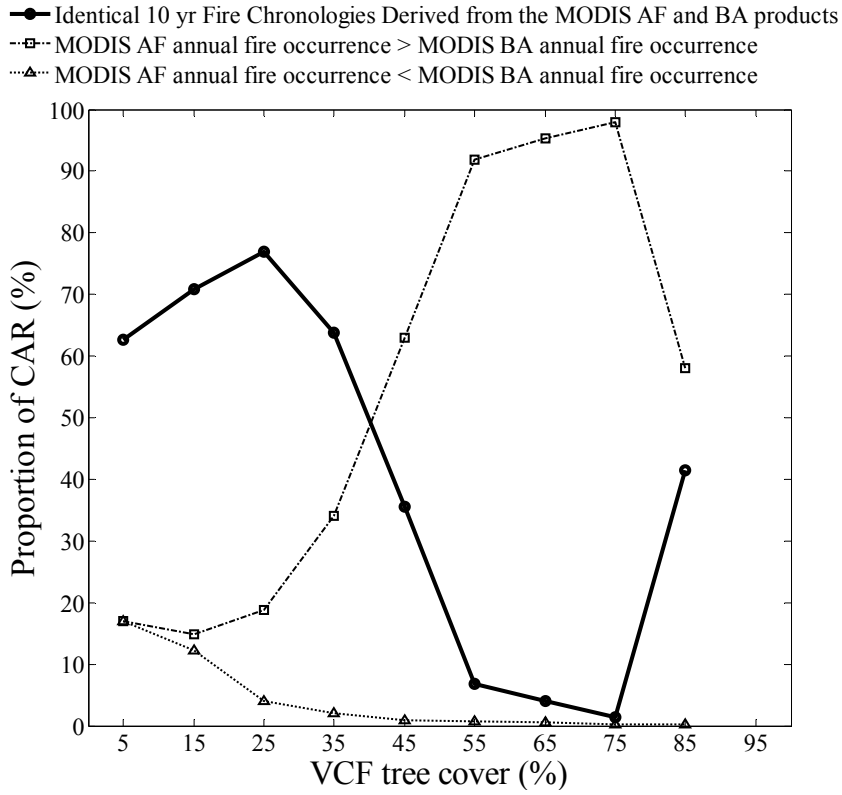

Seasonal profiles of fire activity stratified by tree canopy cover characterized using the Vegetation Continuous Field (VCF) product [59] demonstrate that during the rainy season in mid-July, the few MODIS AF pixel that are detected are equally distributed under the full range of tree canopy cover (Figure 11a). At the start of the dry season in late September, however, MODIS primarily detects AF pixels under sparse tree canopy cover (0%–20%). As the dry season progresses, a greater proportion of MODIS AF pixels are detected under increasing canopy cover, and by the end of March, most MODIS AF pixels are detected under tree canopy cover >60%. Therefore, according to the analysis of the MODIS AF and the VCF products, the fire season in the CAR generally starts and ends earlier under sparse tree canopy cover, and starts and ends later under increased tree canopy cover.

Figure 12a demonstrates that at 0.05° spatial resolution and 16-day temporal resolution, the MCD14ML and WFA products recognize an identical start to the fire season in 20% of the grid cells where both datasets recorded a fire pixel (*i.e.*, $P_{AFAF}^{start} = 0.20$). Where both AF products detected a fire pixel during the study period, both datasets were more likely to yield an identical start to the fire season in the eastern half of the CAR. In the remainder of the grid cells, the MODIS AF product overwhelmingly declares an earlier start to the fire season than the (A)ATSR nighttime AF product. Comparisons between the peak of the fire season derived from the two AF products show similar

patterns, though slightly better agreement (Figure 12b). The best agreement between the MCD14ML and WFA datasets, however, was found at the end of the fire season (Figure 12c) when the two AF products agreed in 48% of the 0.5° grid cells in the CAR (*i.e.*, P_{AFAF}^{end}= 0.48). Again these grid cells were primarily located in the east of the CAR along the border with South Sudan. As the dry season progresses, fuel moistures reach a minimum, and there is greater potential for fires to burn into the night. Given the increased proportion of nighttime fire activity later in the fire season (as evidenced from the MODIS active fire data presented in Figure 11b), the nighttime WFA product is more likely to record these long-duration fires and to better agree with the MCD14ML product at the end of the fire season.

Figure 10. Maps of the (**a**) start; (**b**) peak; (**c**) end; and (**d**) duration of the fire season across the Central African Republic derived by aggregating 10 years of MODIS active fire (AF) pixels at 0.05° grid cell resolution and 16-day temporal resolution.

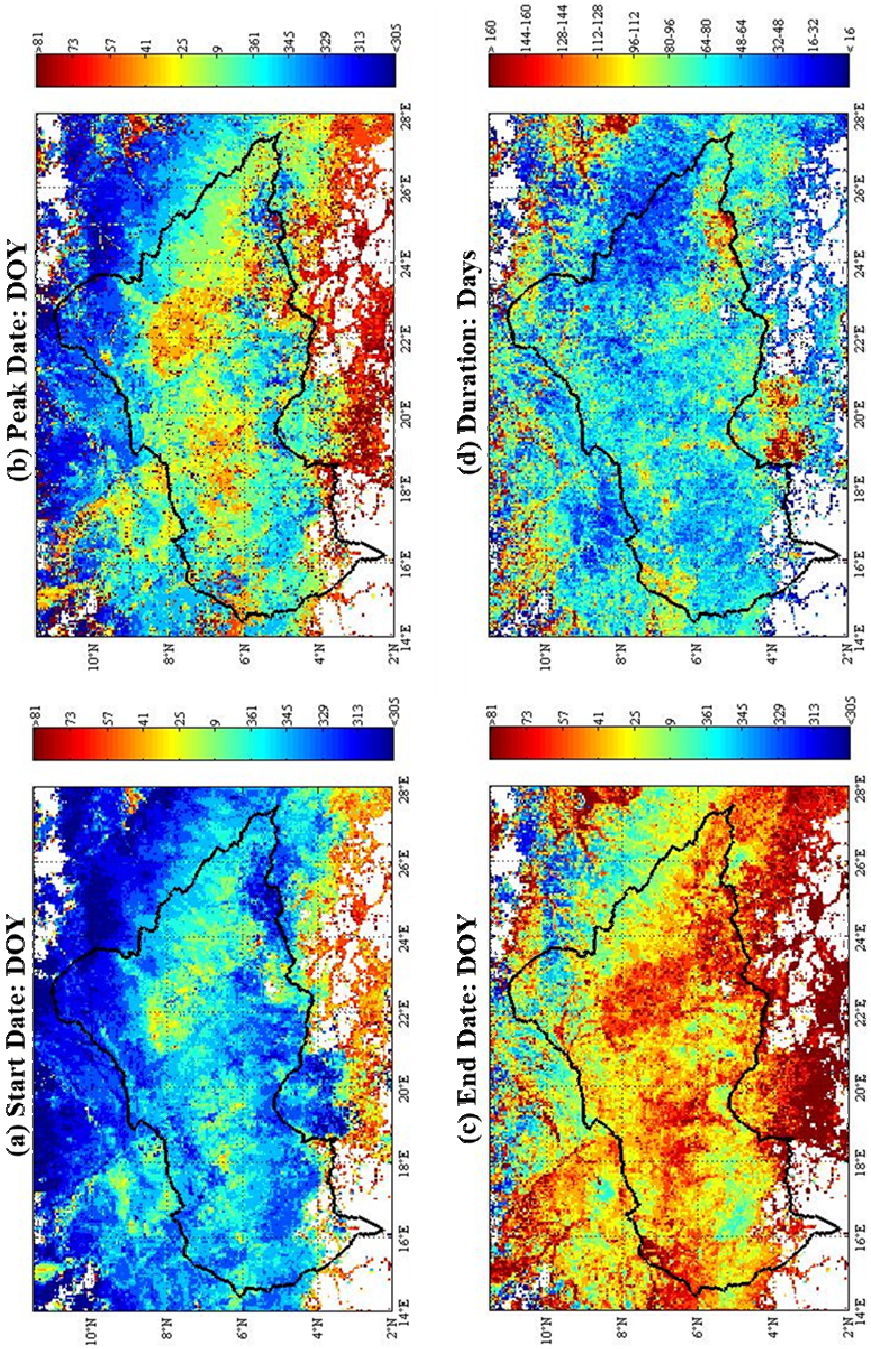

Figure 11. Seasonal profiles of MODIS active fire (AF) pixels detected in the CAR and sorted into 20% intervals of tree canopy cover characterized using the Vegetation Continuous Field (VCF) product [59]. As the dry season progresses (**a**) more MODIS AF pixels are detected under greater canopy cover; and (**b**) a greater proportion of MODIS AF pixels are detected at night.

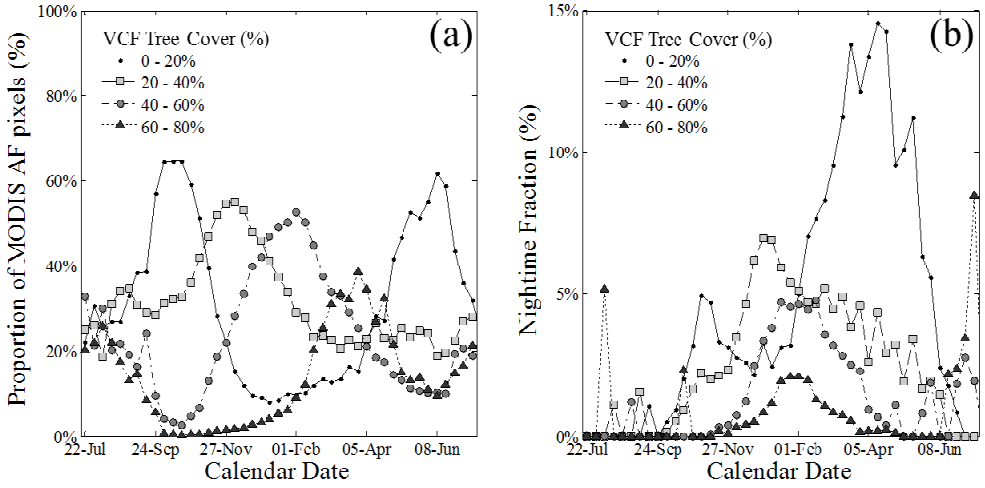

Figure 12. Comparisons of the (**a**) start; (**b**) peak; (**c**) end; and (**d**) duration of the fire season in the Central African Republic (CAR) derived from the MODIS and (A)ATSR active fire (AF) datasets at 16-day temporal resolution. For only the grid cells where both datasets recorded a fire pixel, the value of *P* (triangular symbols) indicates the proportion of grid cells that were assigned an identical start, peak, end or duration by both fire products. Where the fire products disagree, fire seasonality is characterized based on whether MODIS detected an earlier/later or a longer/shorter fire season than (A)ATSR. The proportion of grid cells in the CAR where comparisons were possible are labelled along the top x-axis.

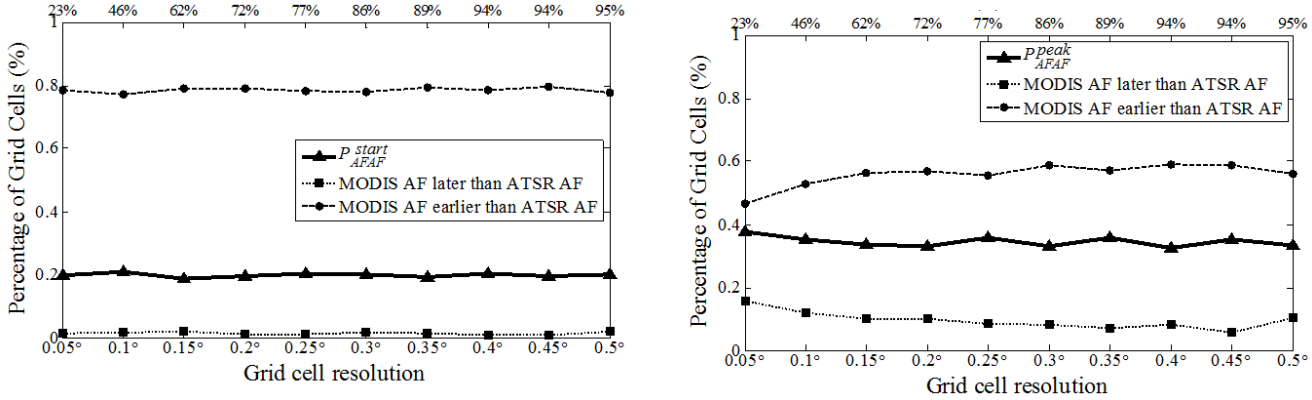

(**a**) (**b**)

Figure 12. *Cont.*

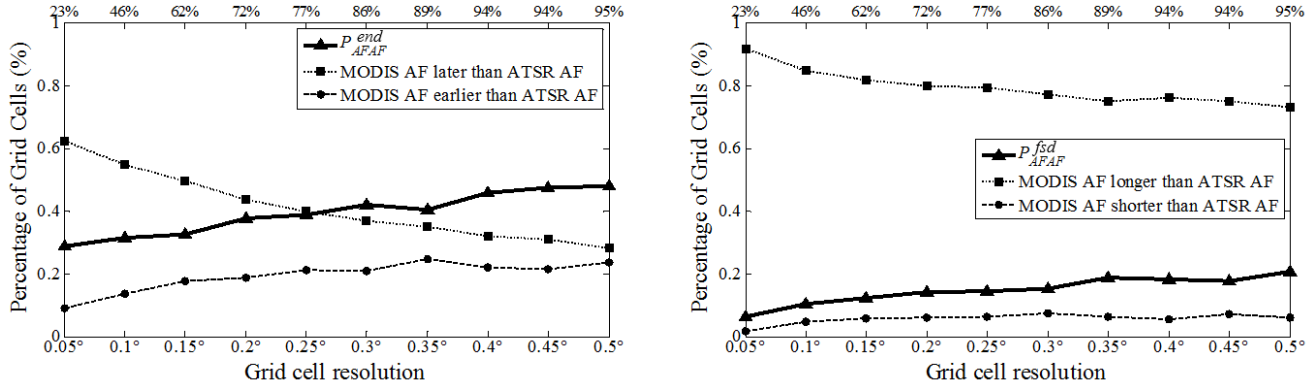

There is very poor agreement between the MODIS and (A)ATSR AF products when characterizing the fire season duration, with P^{fsd}_{AFAF} remaining less than 21% regardless of the grid cell resolution (Figure 12d). Although the agreement between datasets approaches or exceeds ~20% when characterizing either the start *or* the end of the fire season, it is rarer for both datasets yield an identical start *and* end to the fire season for the same grid cell. Hence there is less agreement between the datasets when comparing the fire season duration rather than just comparing either the start or the end of the fire season independently. Coherent with the absence of (A)ATSR fire pixels within fine grid cells, and the predominantly earlier start dates and later end dates identified by MODIS in coarser grid cells, the MODIS AF product estimates a longer fire season duration across the majority of the CAR (Figure 12d).

Unlike comparisons between the two AF products, the MODIS AF and BA datasets provide identical estimates of the onset of the fire season for the majority of the CAR, with $P^{start}_{AFBA} \geq 0.53$ regardless of the grid cell resolution (Figure 13a). Disparities between the AF and BA detection strategies are more evident at the end of the dry season (Figure 13c), however, when the MODIS AF product overwhelmingly declares a later end to the fire season. The contrast in agreement between the start and end of the fire season derived from the AF and BA products is attributed to a coupling between (i) the seasonal location and behavior of fires within the CAR; and (ii) the different remote sensing approaches used to discriminate active fires and burned areas. At the start of the fire season, when active fires are more often detected by MODIS under sparse tree canopy cover (Figure 11a), the signatures of these fires can be relatively well identified using both the AF and BA detection strategies. Later in the fire season, however, as fuels under denser canopy cover dry out and become available to burn, woodlands and forests become susceptible to both new ignitions within the interior as well as the encroachment and penetration by existing savanna fires. Therefore, at the end of the dry season in the CAR, AF detection strategies are better suited for discriminating the thermal radiance emitted from "below-canopy" fires rather than BA detection strategies which, as mentioned previously, rely on the discrimination of sub-canopy changes in surface spectral-reflectance [19,39].

Figure 13. Comparisons of the (**a**) start; (**b**) peak; (**c**) end; and (**d**) duration of the fire season in the Central African Republic (CAR) derived from the MODIS active fire (AF) and burned area (BA) datasets at 16-day temporal resolution. For only the grid cells where both datasets recorded a fire pixel, the value of P (triangular symbols) indicates the proportion of grid cells that were assigned an identical start, peak, end or duration by both fire products. Where the fire products disagree, fire seasonality is characterized based on whether the MODIS active fire product detected an earlier/later or a longer/shorter fire season than the MODIS burned area product. The proportion of grid cells in the CAR where comparisons were possible are labelled along the top x-axis.

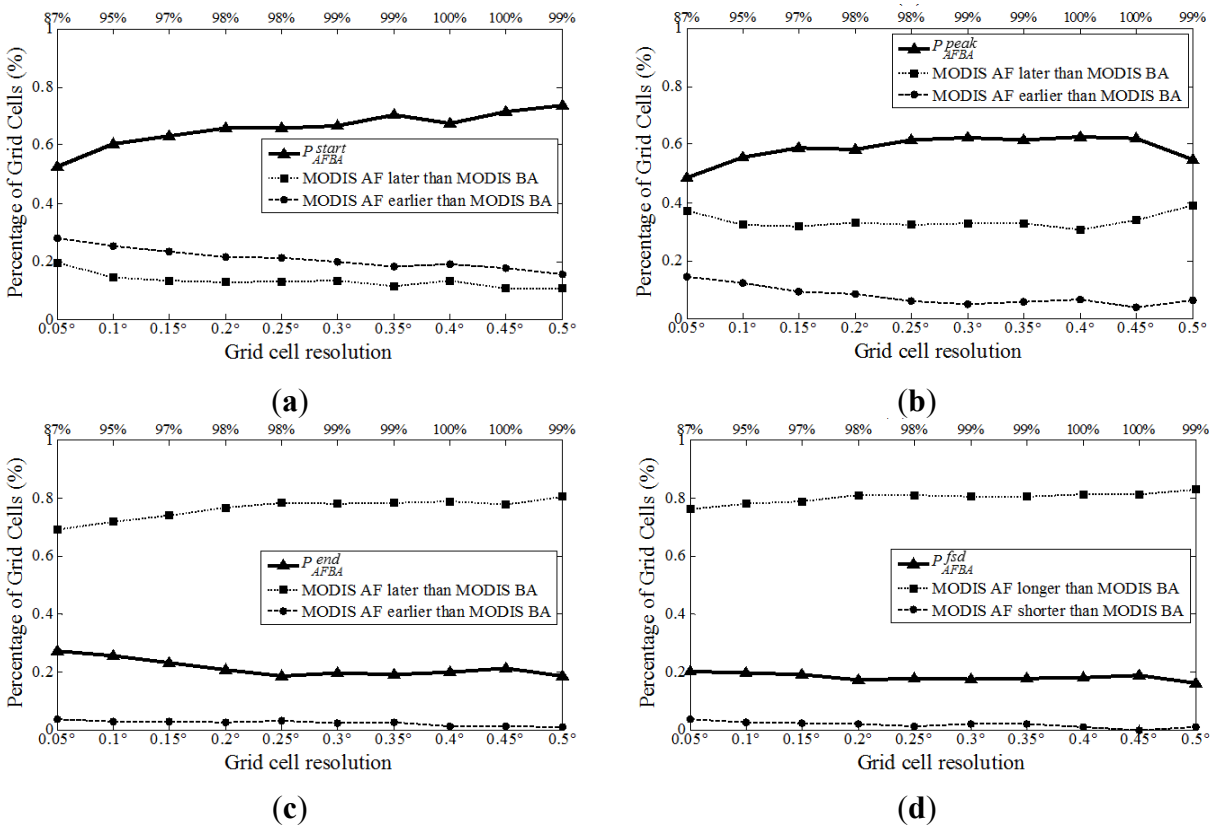

4. Discussion

Agreements between fire regime maps derived from dissimilar datasets were not uniform, but rather varied spatially and temporally depending on a coupling between: (i) the sensor overpass schedule and detection algorithm strategy; and (ii) the characteristic vegetation structure and fire behavior on the landscape. For example, given the nighttime revisit schedule of both sensors and the greater prevalence of nighttime fire activity, the MODIS and (A)ATSR active fire products were more apt to agree in the east of the CAR at the end of the dry season. With unobstructed views of large savanna fires, the MODIS AF and BA products were also more apt to agree in the east of the CAR, but at the beginning of the dry season instead. Superimposed on the geographical gradients and seasonal oscillations, interannual variability and a decreasing decadal trend in the agreement in fire occurrence derived from the three datasets (coinciding with a shift in the measured active fire characteristics and burned area patterns) affected the agreement in fire chronologies. Although it is tempting to suggest that confidence in the

retrieval of fire regime parameters improves where all three maps agree (Figure 6), it cannot be assumed that fires do not occur where none of the datasets recorded a fire pixel.

Results here were restricted to comparisons and interpretations of annual fire occurrence and fire chronologies due to the limitations of confidently estimating fire return intervals and fire frequencies from such brief datasets [53]. Nevertheless, there are some general conclusions that can be drawn from this work. For instance, since MODIS more often detects daytime fire activity burning under increased tree canopy cover, it can be reasoned that the MODIS AF product will yield shorter fire return intervals in the CAR compared to the WFA or MODIS BA products, which in the former case is nighttime-only and in the latter case has problems identifying small, fragmented burned areas under dense canopy cover. It is also worth noting that since it is not possible to determine the spatial distribution of sub-pixel AF and BA components, it can only be assumed that an AF or BA pixel contains evidence that a fire occurred somewhere within the detected pixel. Likewise, grid cells in which the AF and BA pixels were aggregated contain spatially integrated information about fire activity within a given area. Consequently, in this application, fire chronologies derived from gridded AF and BA pixels yield "composite fire intervals" [61]. If fire sizes are small relative to the grid cell size in which the AF and BA pixels are aggregated, then the composite fire interval will decrease as the grid cell size increases. Conversely, if fire sizes are larger than the grid cell resolution, then the composite fire interval will remain constant as the grid cell size increases. This scale dependence is well-studied and is referred to as the interval-area relationship [62,63]. Given the geographical differences in fire behavior, it is expected that a gradient of interval-area relationships exists across the CAR. For example, in the west, as grid cells expand to encompass a greater number of AF and BA pixels associated with smaller agricultural fires, the improved agreement between the MODIS AF and BA-derived fire chronologies will coincide with a decrease in the composite fire interval. In the east of the CAR, however, the agreement between the MODIS AF and BA- derived fire chronologies will yield identical composite fire intervals that are not expected to change as the grid cell size increases around the extremely long and continuous fire fronts in the region.

Aside from the composite fire interval, there are other options for calculating an area-based fire return interval. For example, Moritz *et al.* [53] assigned fire return intervals to grid cells based on the fire return interval measured at the center of the grid cell, and Parsons *et al.* [64] pooled all samples of point-based fire return intervals over an entire grid cell. Whilst it is possible to process satellite-based AF and BA pixels to derive an area-based fire return interval similar to Moritz *et al.* [53] or Parsons *et al.* [64], each of these calculations has a different physical meaning that, while beyond the scope of this work, should be carefully considered when interpreting satellite-based fire regime maps.

The MODIS AF product predominantly identified earlier start dates, later end dates, and longer fire season durations in the CAR compared to the (A)ATSR WFA and the MODIS BA products. As with fire chronologies, characterizing fire seasonality from satellite-based AF and BA pixels is also scale dependent. Here seasonal profiles were generated for each grid cell based on an aggregation of 10 years of AF or BA pixels. As such, the start and end of the fire season derived in this work represents the earliest and latest possible dates (*i.e.*, the seasonal burn window) during the decade when: (i) natural and/or anthropogenic ignitions occurred on the landscape; and (ii) fuel conditions were able to support a spreading fire. If instead the seasonal profile in a grid cell is generated from a single year of fire pixels, then the fire season determined in this manner may only encompass an isolated event that

occurred at a discrete time within the possible burn window. Thus, we expect fire season durations to increase as aggregated temporal profiles are constructed from AF and BA pixels accumulated over a greater number of years. Similarly, since seasonal profiles of fire pixels within fine grid cells may also represent isolated fire events, we expect fire season durations to increase as the grid cell size increases to include multiple fire events captured across broader areas. A preliminary analysis of the sensitivity of the fire season duration to grid cell size indicates this to be true (Figure 14), however we concede that this scale-dependent response may not be universal, but rather linked to the method used to define the fire season duration (*i.e.*, see next paragraph). Future work should address issues of spatial and temporal scale, and, in particular, should examine the as of yet unexplained relationships between the sensor-to-sensor agreement in fire seasonality and grid cell resolution (Figures 12 and 13).

Figure 14. Preliminary results supporting our assertion that the characterization of fire season durations in the CAR would increase if fire pixels are accumulated into coarser grid cells. Distributions are constructed using MODIS active fire pixels only.

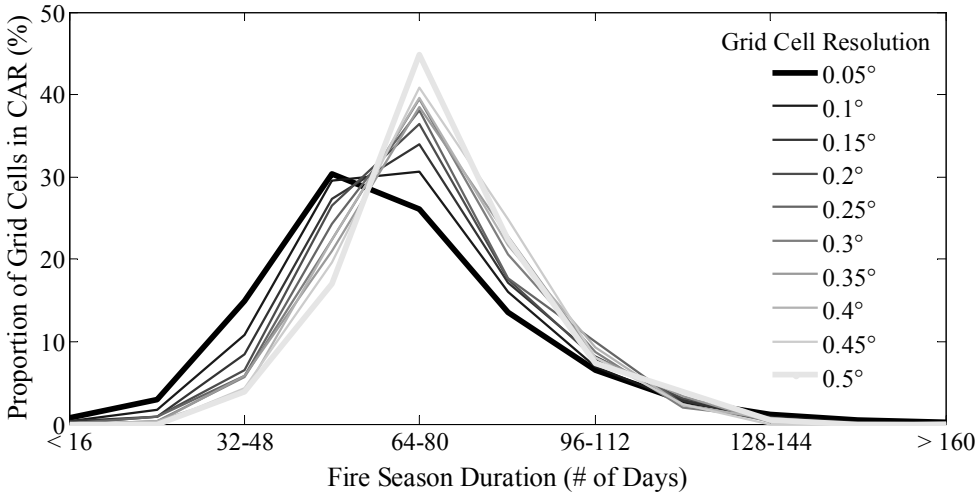

Identifying fire arrival and extinction times based on the 10th and 90th percentiles of the cumulative distribution of fire detections, as performed here, essentially brackets the continuous time of year that an area experiences the majority of fire activity. This description of the fire season assumes that fuels within the grid cell, if not already burned, are flammable between the start and end dates even if ignitions are lacking and fires are absent. There are a variety of other options for characterizing the fire season besides this definition. For example, the fire season duration (as calculated here) is longer than the "core fire season" [27,28] calculated based on the 25th/75th percentiles, and is also typically longer than the "length of fire period" [25] calculated by applying fixed thresholds to fire pixel counts or fire pixel densities. Again, each of these parameters are derived differently from satellite-based fire products, and each has a different physical meaning that, while beyond the scope of this work, should be considered when using AF and BA pixels to interpret fire seasonality.

Spatial and temporal discrepancies in fire regime parameters derived from different satellite-based fire products will inevitably confound assessments of the vegetative, climatic, and anthropogenic drivers of fire activity. Furthermore, disagreements in fire regime parameters derived from different satellite-based fire products raises concerns over which satellite-based fire product is most appropriate for constructing, constraining, and evaluating the myriad of statistical models and long-term landscape

fire simulations designed to summarize and/or mimic fire regimes. In the crudest sense, if satellite fire products cannot themselves provide a consistent set of fire regime parameters, then modellers should be wary of tuning their models to agree too strongly with information from one particular product. Instead we echo the suggestions of Morgan *et al.* [1] and recommend characterizing fire regime parameters using an integrated approach to assimilate information from multiple fire products (e.g., [19]).

Publically available satellite-based fire products that provide global coverage currently span a decade (in the case of MODIS) or longer (in the case of the (A)ATSR series). Satellite records will continue to grow as fire products are generated from new and future missions, such as NPP VIIRS [65] and Sentinel-3 SLSTR [66]. Although truncation and censorship [10,53] affect the confidence in the retrieval of fire regime parameters, we argue that as the archives continue to grow, a decade of observations can be used to represent a "snapshot" of a dynamic fire regime. Therefore, we suggest that there are other more pressing issues associated with deriving fire regimes from satellite observations besides the record duration, namely (i) the disagreements that arise when fire regime parameters are derived from dissimilar datasets; (ii) the scale dependent relationships and interpretations that arise when more and more years of AF and BA pixels are aggregated into grid cells of various sizes; and (iii) the numerous methods available to derive a variety of fire regime parameters that are sometimes created "ad-hoc" to accommodate the limitations of satellite observations, and the often ambiguous link between these remote sensing variables and their underlying physical meaning.

5. Conclusions

Active fire (AF) and burned are (BA) pixels detected by the Moderate Resolution Imaging Spectroradiometer (MODIS) and Along Track Scanning Radiometer (ATSR) have typically been compared at the pixel level and on an instantaneous or daily basis. This work has extended such studies, and for the first time has directly examined the ability of three widely used datasets to provide competing and/or synergistic descriptions of individual fire regime parameters (e.g., fire chronologies and fire seasonality) over a broad range of spatial and temporal scales. Key findings specific to the Central African Republic (CAR) and other locations with similar fire regimes are summarized here:

- Annual fire occurrence maps derived from the different datasets exhibited the poorest agreement at the finest 0.05° grid cell resolution where the MODIS and ATSR AF products agreed across no more than 13% of the CAR, and the MODIS AF and BA products agreed across no more than 80% of the CAR;
- Annual fire occurrence maps were more coherent as grid cells were expanded, and exhibited the best agreement at the coarsest 0.5° spatial resolution where the MODIS and ATSR AF products agreed across no less than 63% of the CAR, and the MODIS AF and BA products displayed near perfect agreement;
- Map agreements of annual fire occurrence derived from the dissimilar fire products decreased (by upwards of 20%) from the beginning to the end of the study period due to an observed shift in active fire characteristics and burned area patterns;
- Due to decreasing trends and interannual variability in the detection of annual fire occurrence, the agreement in fire chronologies derived from dissimilar fire products diminished as the number of years included in the time series increased. After 10 years, for example, at 0.05°

spatial resolution, map agreements between the MODIS and ATSR AF-derived fire chronologies reduced to less than 1%, and map agreements between the MODIS AF- and BA-derived fire chronologies reduced to ~41%;

- All three datasets provided distinctly different portraits of the onset, peak, and duration of the fire season regardless of map resolution, with the MODIS AF product predominantly identifying an earlier start date and a later end date compared to the ATSR AF and the MODIS BA products.

Given the discrepancies found here, we caution against using a single active fire or burned area product to describe a fire regime. Instead we recommend characterizing fire regime parameters using an integrated approach designed to assimilate information from multiple satellite-based fire products. Nevertheless, since different satellite sensors and detection algorithm strategies are sensitive to different types of fires, we've demonstrated here for the first time that disagreements in fire regime maps derived from dissimilar satellite-based fire products can be used to identify spatial and temporal transitions in landscape fire activity. For instance, we highlight a decadal shift towards smaller and lower intensity fires in the CAR. In this regard, we suggest that future work examine whether discrepancies between dissimilar satellite-based fire products can be used to inform traditional descriptions of fire regimes and/or to identify other regions with shifting fire regimes.

Acknowledgments

The authors kindly thank three anonymous reviewers and the editor for their very helpful comments. NASA is acknowledged for free access to MODIS data, and ESA is acknowledged for access to the WFA. P.H.F. was partially funded through a King's College London (SSPP) studentship award, M.A.C. was supported by a NASA Interdisciplinary Sciences grant (NNX11AB89G), and M.J.W. was funded by the UK National Centre for Earth Observation.

Author Contributions

Patrick H. Freeborn designed the study, analyzed the data, and wrote the manuscript. Mark A. Cochrane and Martin J. Wooster contributed to the study design and to the writing of the manuscript.

Conflicts of Interest

The authors declare no conflict of interest.

References

1. Morgan, P.; Hardy, C.; Swetnam, T.; Rollins, M.; Long, D. Mapping fire regimes across time and space: Understanding coarse and fine-scale fire patterns. *Int. J. Wildland Fire* **2001**, *10*, 329–342.
2. Hardy, C.; Schmidt, K.; Menakis, J.; Sampson, R. Spatial data for national fire planning and fuel management. *Int. J. Wildland Fire* **2001**, *10*, 353–372.
3. Rollins, M.; Keane, R.; Parsons, R. Mapping fuels and fire regimes using remote sensing, ecosystem simulation, and gradient modeling. *Ecol. Appl.* **2004**, *14*, 75–95.
4. Krebs, P.; Pezzatti, G.; Mazzoleni, S.; Talbot, L.; Conedera, M. Fire regime: History and definition of a key concept in disturbance ecology. *Theory Biosci.* **2010**, *129*, 53–69.

5. Power, M.; Marlon, J.; Bartlein, P.; Harrison, S. Fire history and the Global Charcoal Database: A new tool for hypothesis testing and data exploration. *Palaeogeogr. Palaeoclimatol. Palaeoecol.* **2010**, *291*, 52–59.
6. Falk, D.; Heyerdahl, E.; Brown, P.; Farris, C.; Fule, P.; McKenzie, D.; Swetnam, T.; Taylor, A.; van Horne, M. Multi-scale controls of historical forest-fire regimes: New insights from fire-scar networks. *Front. Ecol. Environ.* **2011**, *9*, 446–454.
7. Brown, T.J.; Hall, B.L.; Mohrle, C.R.; Reinbold, H.J. *Coarse Assessment of Federal Wildland Fire Occurrence Data*; Program for Climate, Ecosystem and Fire Applications, Desert Research Institute: Reno, NV, USA, 2002; p. 30.
8. Gibson, C.E.; Morgan, P. *Atlas of Digital Polygon Fire Extents for Idaho and Western Montana (1889–2003)*; USDA Forest Service, Rocky Mountain Research Station: Fort Collins, CO, USA, 2009.
9. Morgan, P.; Bunting, S.; Black, A.; Merrill, T.; Barrett, S.; Wright, R.G. *Fire Regimes in the Interior Columbia River Basin: Past and Present*; Final Report for RJVA-INT-94913; Intermountain Fire Sciences Laboratory Lntermountain Research Station: Missoula, MT, USA, 1996.
10. Johnson, E.A.; Gutsell, S.L. Fire frequency models, methods and interpretations. *Adv. Ecol. Res.* **1994**, *25*, 239–287.
11. Keane, R.; Cary, G.; Parsons, R. Using simulation to map fire regimes: An evaluation of approaches, strategies, and limitations. *Int. J. Wildland Fire* **2003**, *12*, 309–322.
12. Keane, R.; Cary, G.; Davies, I.; Flannigan, M.; Gardner, R.; Lavorel, S.; Lenihan, J.; Li, C.; Rupp, T. A classification of landscape fire succession models: Spatial simulations of fire and vegetation dynamics. *Ecol. Model.* **2004**, *179*, 3–27.
13. McKenzie, D.; Peterson, D.L.; Alvarado, E. Extrapolation problems in modeling fire effects at large spatial scales: A review. *Int. J. Wildland Fire* **1996**, *6*, 165–176.
14. Roy, D.P.; Boschetti, L.; Smith, A.M.S. Satellite Remote Sensing of Fires. In *Fire Phenomena and the Earth System: An Interdisciplinary Guide to Fire Science*; Belcher, C.M., Ed.; John Wiley & Sons, Ltd.: Chichester, UK, 2013; pp. 77–96.
15. Giglio, L.; Descloitres, J.; Justice, C.; Kaufman, Y. An enhanced contextual fire detection algorithm for MODIS. *Remote Sens. Environ.* **2003**, *87*, 273–282.
16. Arino, O.; Casadio, S.; Serpe, D. Global night-time fire season timing and fire count trends using the ATSR instrument series. *Remote Sens. Environ.* **2012**, *116*, 226–238.
17. Roy, D.; Lewis, P.; Justice, C. Burned area mapping using multi-temporal moderate spatial resolution data—A bi-directional reflectance model-based expectation approach. *Remote Sens. Environ.* **2002**, *83*, 263–286.
18. Archibald, S.; Scholes, R.; Roy, D.; Roberts, G.; Boschetti, L. Southern African fire regimes as revealed by remote sensing. *Int. J. Wildland Fire* **2010**, *19*, 861–878.
19. Devineau, J.; Fournier, A.; Nignan, S. Savanna fire regimes assessment with MODIS fire data: Their relationship to land cover and plant species distribution in western Burkina Faso (West Africa). *J. Arid Environ.* **2010**, *74*, 1092–1101.
20. Alencar, A.; Asner, G.; Knapp, D.; Zarin, D. Temporal variability of forest fires in eastern Amazonia. *Ecol. Appl.* **2011**, *21*, 2397–2412.

21. Oliveira, S.; Pereira, J.; Carreiras, J. Fire frequency analysis in Portugal (1975–2005), using Landsat-based burnt area maps. *Int. J. Wildland Fire* **2012**, *21*, 48–60.
22. Giglio, L.; Csiszar, I.; Justice, C. Global distribution and seasonality of active fires as observed with the Terra and Aqua Moderate Resolution Imaging Spectroradiometer (MODIS) sensors. *J. Geophys. Res.: Biogeosci.* **2006**, *111*, doi:10.1029/2005JG000142.
23. Gregoire, J.; Pinnock, S.; Dwyer, E.; Janodet, E. Satellite monitoring of vegetation fires for EXPRESSO: Outline of activity and relative importance of the study area in the global picture of biomass burning. *J. Geophys. Res.: Atmos.* **1999**, *104*, 30691–30699.
24. Dwyer, E.; Pereira, J.M.C.; Gregoire, J.M.; DaCamara, C.C. Characterization of the spatio-temporal patterns of global fire activity using satellite imagery for the period April 1992 to March 1993. *J. Biogeogr.* **2000**, *27*, 57–69.
25. Chuvieco, E.; Giglio, L.; Justice, C. Global characterization of fire activity: Toward defining fire regimes from Earth observation data. *Glob.Chang. Biol.* **2008**, *14*, 1488–1502.
26. Nielsen, T. Characterization of fire regimes in the Experiment for Regional Sources and Sinks of Oxidants (EXPRESSO) Study Area. *J. Geophys. Res.: Atmos.* **1999**, *104*, 30713–30723.
27. Giglio, L. Characterization of the tropical diurnal fire cycle using VIRS and MODIS observations. *Remote Sens. Environ.* **2007**, *108*, 407–421.
28. Gregoire, J.M.; Simonetti, D. Interannual changes of fire activity in the protected areas of the SUN Network and other parks and reserves of the West and Central Africa region derived from MODIS observations. *Remote Sens.* **2010**, *2*, 446–463.
29. Bucini, G.; Lambin, E.F. Fire impacts on vegetation in Central Africa: A remote-sensing-based statistical analysis. *Appl. Geogr.* **2002**, *22*, 27–48.
30. Lambin, E.F.; Goyvaerts, K.; Petit, C. Remotely-sensed indicators of burning efficiency of savannah and forest fires. *Int. J. Remote Sens.* **2003**, *24*, 3105–3118.
31. Clerici, N.; Boschetti, L.; Eva, H.; Grégoire, J.M. Assessing Vegetation Fires Activity and Its Drivers in West-Central Africa Using MODIS and TRMM Data. In Proceedings of the 2004 IEEE International Geoscience and Remote Sensing Symposium, Anchorage, AK, USA, 20–24 September 2004.
32. Archibald, S.; Lehmann, C.E.R.; Gomez-Dans, J.L.; Bradstock, R.A. Defining pyromes and global syndromes of fire regimes. *Proc. Natl. Acad. Sci. USA* **2013**, *110*, 6442–6447.
33. Morisette, J.; Giglio, L.; Csiszar, I.; Setzer, A.; Schroeder, W.; Morton, D.; Justice, C. Validation of MODIS active fire detection products derived from two algorithms. *Earth Interact.* **2005**, *9*, 1–25.
34. Morisette, J.; Giglio, L.; Csiszar, I.; Justice, C. Validation of the MODIS active fire product over Southern Africa with ASTER data. *Int. J. Remote Sens.* **2005**, *26*, 4239–4264.
35. Csiszar, I.A.; Morisette, J.T.; Giglio, L. Validation of active fire detection from moderate-resolution satellite sensors: The MODIS example in northern Eurasia. *IEEE Trans. Geosci. Remote Sens.* **2006**, *44*, 1757–1764.
36. Schroeder, W.; Prins, E.; Giglio, L.; Csiszar, I.; Schmidt, C.; Morisette, J.; Morton, D. Validation of GOES and MODIS active fire detection products using ASTER and ETM plus data. *Remote Sens. Environ.* **2008**, *112*, 2711–2726.
37. Boschetti, L.; Roy, D.; Justice, C.; Giglio, L. Global assessment of the temporal reporting accuracy and precision of the MODIS burned area product. *Int. J. Wildland Fire* **2010**, *19*, 705–709.

38. Roberts, G.; Wooster, M.; Freeborn, P.H.; Xu, W. Integration of geostationary FRP and polar-orbiter burned area datasets for an enhanced biomass burning inventory. *Remote Sens. Environ.* **2011**, *115*, 2047–2061.
39. Roy, D.; Boschetti, L.; Justice, C.; Ju, J. The collection 5 MODIS burned area product—Global evaluation by comparison with the MODIS active fire product. *Remote Sens. Environ.* **2008**, *112*, 3690–3707.
40. Freeborn, P.H.; Wooster, M.J.; Roberts, G.; Xu, W. Evaluating the SEVIRI fire thermal anomaly detection algorithm across the Central African Republic using the MODIS active fire product. *Remote Sens.* **2014**, *6*, 1890–1917.
41. Barbosa, P.M.; Stroppiana, D.; Gregoire, J.M.; Pereira, J.M.C. An assessment of vegetation fire in Africa (1981–1991): Burned areas, burned biomass, and atmospheric emissions. *Glob. Biogeochem. Cy.* **1999**, *13*, 933–950.
42. Eva, H.; Lambin, E. Burnt area mapping in Central Africa using ATSR data. *Int. J. Remote Sens.* **1998**, *19*, 3473–3497.
43. Brivio, P.A.; Maggi, M.; Binaghi, E.; Gallo, I. Mapping burned surfaces in sub-Saharan Africa based on multi-temporal neural classification. *Int. J. Remote Sens.* **2003**, *24*, 4003–4018.
44. Justice, C.O.; Vermote, E.; Townshend, J.R.G.; Defries, R.; Roy, D.P.; Hall, D.K.; Salomonson, V.V.; Privette, J.L.; Riggs, G.; Strahler, A.; *et al.* The moderate resolution imaging spectroradiometer (MODIS): Land remote sensing for global change research. *IEEE Trans. Geosci. Remote Sens.* **1998**, *36*, 1228–1249.
45. Kaufman, Y.; Herring, D.; Ranson, K.; Collatz, G., Earth Observing System AM1 mission to earth. *IEEE Trans. Geosci. Remote Sens*. **1998**, doi:10.1109/36.700989.
46. Parkinson, C. Aqua: An earth-observing satellite mission to examine water and other climate variables. *IEEE Trans. Geosci. Remote Sens.* **2003**, *41*, 173–183.
47. Kaufman, Y.; Justice, C.; Flynn, L.; Kendall, J.; Prins, E.; Giglio, L.; Ward, D.; Menzel, W.; Setzer, A. Potential global fire monitoring from EOS-MODIS. *J. Geophys. Res.: Atmos.* **1998**, *103*, 32215–32238.
48. Justice, C.; Giglio, L.; Korontzi, S.; Owens, J.; Morisette, J.; Roy, D.; Descloitres, J.; Alleaume, S.; Petitcolin, F.; Kaufman, Y. The MODIS fire products. *Remote Sens. Environ.* **2002**, *83*, 244–262.
49. Giglio, L. *MODIS Collection 5 Active Fire Product User's Guide: Version 2.5*; Department of Geographical Sciences University of Maryland: College Park, MD, USA, 2013.
50. Rasmussen, K.; Russell-Smith, J.; Morisette, J.T. Establishing Validation Site Network for Remote Sensing Applications to Fire Research: A Joint Activity Between GOFC-Fire and the LPV Subgroup. Available online: http://lpvs.gsfc.nasa.gov/PDF/GOFC_LPV_fire_sites.pdf (accessed on 28 April 2014).
51. Delmas, R.; Druilhet, A.; Cros, B.; Durand, P.; Delon, C.; Lacaux, J.; Brustet, J.; Serca, D.; Affre, C.; Guenther, A.; *et al.* Experiment for regional sources and sinks of oxidants (EXPRESSO): An overview. *J. Geophys. Res.: Atmos.* **1999**, *104*, 30609–30624.
52. Pereira, J.M.C.; Pereira, B.S.; Barbosa, P.; Stroppiana, D.; Vasconcelos, M.J.P.; Gregoire, J.M. Satellite monitoring of fire in the EXPRESSO study area during the 1996 dry season experiment: Active fires, burnt area, and atmospheric emissions. *J. Geophys. Res.: Atmos.* **1999**, *104*, 30701–30712.

53. Moritz, M.A.; Moody, T.J.; Miles, L.J.; Smith, M.M.; de Valpine, P. The fire frequency analysis branch of the pyrostatistics tree: Sampling decisions and censoring in fire interval data. *Environ. Ecol. Stat.* **2009**, *16*, 271–289.
54. Eva, H.; Flasse, S. Contextual and multiple-threshold algorithms for regional active fire detection with AVHRR data. *Remote Sens. Rev.* **1996**, *14*, 333–351.
55. Roberts, G.; Wooster, M.; Lagoudakis, E. Annual and diurnal african biomass burning temporal dynamics. *Biogeosciences* **2009**, *6*, 849–866.
56. Giglio, L.; Randerson, J.T.; van der Werf, G.R., Analysis of daily, monthly, and annual burned area using the fourth-generation global fire emissions database (GFED4). *J. Geophys. Res.: Biogeosci*. **2013**, *118*, 317–328.
57. Giglio, L.; Loboda, T.; Roy, D.; Quayle, B.; Justice, C., An active-fire based burned area mapping algorithm for the MODIS sensor. *Remote Sens. Environ*. **2009**, *113*, 408–420.
58. Brncic, T.M.; Willis, K.J.; Harris, D.J.; Telfer, M.W.; Bailey, R.M. Fire and climate change impacts on lowland forest composition in Northern Congo during the last 2580 years from palaeoecological analyses of a seasonally flooded swamp. *Holocene* **2009**, *19*, 79–89.
59. Hansen, M.C.; DeFries, R.S.; Townshend, J.R.G.; Carroll, M.; Dimiceli, C.; Sohlberg, R.A. Global percent tree cover at a spatial resolution of 500 meters: First results of the MODIS vegetation continuous fields algorithm. *Earth Interact.* **2003**, *7*, 1–15.
60. Koffi, B.; Gregoire, J.M.; Mahe, G.; Lacaux, J.P. Remote-sensing of Bush Fire dynamics in Central-Africa from 1984 to 1988—Analysis in relation to regional vegetation and pluviometric patterns. *Atmos. Res.* **1995**, *39*, 179–200.
61. Dieterich, J.H. The Composite Fire Interval—A Tool for More Accurate Interpretation of Fire History. In Proceedings of the Fire History Workshop, Tucson, AZ, USA, 20–24 October 1980; pp. 8–14.
62. Falk, D.; Miller, C.; McKenzie, D.; Black, A. Cross-scale analysis of fire regimes. *Ecosystems* **2007**, *10*, 809–823.
63. McKenzie, D.; Kennedy, M. Scaling Laws and Complexity in Fire Regimes. In *The Landscape Ecology of Fire*; McKenzie, D., Miller, C., Falk, D.A., Eds.; Springer Ltd.: Dordrecht, The Netherlands, 2011; pp. 27–49.
64. Parsons, R.; Heyerdahl, E.; Keane, R.; Dorner, B.; Fall, J. Assessing accuracy of point fire intervals across landscapes with simulation modelling. *Can. J. For. Res.* **2007**, *37*, 1605–1614.
65. Justice, C.O.; Roman, M.O.; Csiszar, I.; Vermote, E.F.; Wolfe, R.E.; Hook, S.J.; Friedl, M.; Wang, Z.; Schaaf, C.B.; Miura, T.; *et al.* Land and cryosphere products from Suomi NPP VIIRS: Overview and status. *J. Geophys. Res.: Atmos.* **2013**, *118*, 9753–9765.
66. Wooster, M.J.; Xu, W.; Nightingale, T. Sentinel-3 SLSTR active fire detection and FRP product: Pre-launch algorithm development and performance evaluation using MODIS and ASTER datasets. *Remote Sens. Environ.* **2012**, *120*, 236–254.